

Two-dimensional CVD Profile Simulator Based on Ballistic Transport and Reaction Model

Takuya Maruizumi, Yoshiaki Takemura, Jiro Ushio, and Masanobu Miyao

Central Research Laboratory, Hitachi, Ltd., Kokubunji-shi, Tokyo 185-8601, Japan
Phone: +81-42-323-1111, Fax: +81-42-327-7748, E-mail: marui@crl.hitachi.co.jp

1. Introduction

Various chemical vapor deposition (CVD) processes have been developed over the last 20 years and several have become established as fundamental film-deposition techniques for ULSI applications. The ongoing need to enlarge wafer size and shrink device size continues to stimulate the demand for accurate CVD simulation at both the micro-device-feature level and at the reactor-scale level in order to determine the process conditions for uniform deposition without having to conduct trial-and-error experiments. Several approaches for feature-scale simulation have been developed to predict the step-coverage characteristics of low-pressure CVD, in which the molecular flow must be solved simultaneously with complicated chemical reactions [1-4]. Among these approaches, the Monte Carlo scheme and the ballistic transport and reaction model (BTRM) scheme, in which the deposition reaction is commonly characterized by a single parameter (the reactive sticking coefficient) have achieved reasonable success in profile prediction. The reactive sticking coefficient, σ , is defined as the ratio of the number of molecules of species i that become part of film R_i per area per unit of time to the total number of impinging molecules, η_i , per area per unit of time:

$$\sigma = R_i / \eta_i \quad (1)$$

From this definition of the reactive sticking coefficient, it follows that the larger the sticking coefficient, the lower the flux leaving the surface and the lower the expected step coverage [5]. Several simulation results have been reported in which the film conformality improved as the sticking coefficient of the reactant gas was reduced from unity to small decimal amount [4,6]. The idea of the reactive sticking coefficient is so sophisticated that it enabled complicated deposition chemistry to be finely modeled and extended beyond first-order reaction kinetics. However, whether the reactive sticking coefficient can be generally used as a determinant descriptor for the step-coverage characteristics of CVD has not been clarified.

In this paper we will show that although the reactive sticking coefficient can be used to simulate the deposition profile, it is inadequate for evaluating the step-coverage characteristics. We do this by simulating the profiles of seven CVD processes. We use the BTRM approach developed by Cale et al. because any deposition mechanism can be modeled by using the general reactive sticking coefficient defined in Eq. (1).

2. Feature-scale Deposition Simulator

We have extended two-dimensional deposition simulator with a micrometer-feature-scale originally developed by Cale et al. to include a scheme to inhibit and/or accelerate the deposition reactions stemming from the product gases [4]. We also improved the algorithm used to attain a self-consistent gas flux distribution over the micro feature shape at each step in the simulation. To clarify these points, we briefly describe our deposition simulator and flux-distribution algorithm below.

The originally proposed governing equation for flux distribution η_i^a on a feature shape is given by Eq. (2), where film b is assumed to be formed from the reaction of source gas a . The subscripts i, j , and v mean line segment i, j on the feature shape and source volume, respectively.

$$\eta_i^a = q_{iv} \eta_v^a + \sum_{j=i} (1 - \sum_b S_j^{ab}) \eta_j^a q_{ij} l_j \quad (2)$$

where S_j^{ab} is the position-dependent reactive sticking probability defined in Eq. (1) and q_{ij} is the transmission probability reflecting the geometrical relation between segments i and j (Fig. 1). The detailed formulation of this equation and the assumptions are described in the original paper [4]. The first term on the right-hand side of Eq. (2) is the gas flux impinging on element i from the source volume, and the second term is the flux ejected from all other line segments to segment i . Equation (2) thus describes the flux balance at each segment on the feature shape. Unfortunately, it is difficult to describe the effect of the product gas, i.e., the acceleration and/or inhibition of the film-forming reaction, with this equation. This problem can be solved straightforwardly by introducing another term to account for the reactions caused by the product gas:

$$\text{added term} = \sum_{j=i} \sum_c S_j^{ca} \eta_j^c (n_a/n_c) l_j \quad (3)$$

where S_j^{ca} is the reactive sticking coefficient of product gas c

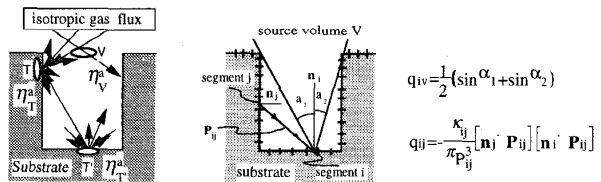


Fig. 1 The definition of flux η , segment i , and transmission probability q_{ij} on a feature shape.

to form source gas a, and n_a and n_c are the stoichiometric coefficients for the corresponding reactions of the product gas. Adding Eq. (3) to Eq. (2) produces a simultaneous linear equation with respect to flux distribution η_1^a that can be readily solved by using the normal program libraries. The deposition simulation algorithm is shown in Fig. 2. The simulator has three primary routines. The first is a feature-shape discretization routine, the second is a flux-solving routine, and the third is a profile-evolution routine. The main routine solves the flux distribution on feature shape by using the governing equation given by Eqs. (2) and (3). Because this equation contains reactive sticking coefficients S^{ab}_j , which depend on the local flux distribution on the feature shape, a self-consistent solution is needed. This point is not explicitly considered in the literature. Solving steps 5 to 8 is an iteration routine that produce a self-consistent solution. To avoid both divergence and oscillation problems, a mixing procedure for successive solutions is used. The mixing ratio was empirically optimized with respect to

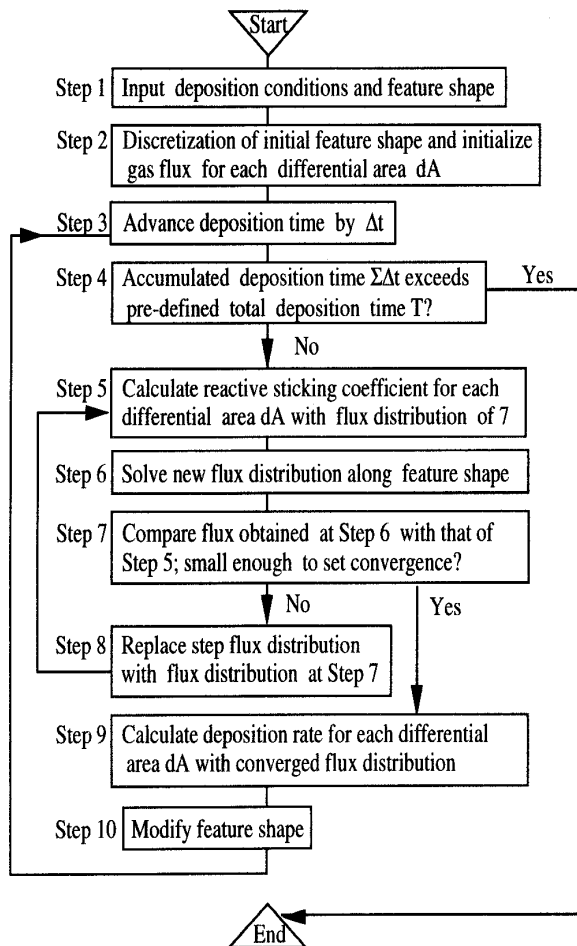


Fig. 2 Flow chart for the film-deposition simulation algorithm based on ballistic transport and reaction model. To attain a self-consistent solution, a flux convergence loop, step 5 to 8, was added to the original algorithm.

the total number of iterations. We extensively applied this profile simulator to seven kinds of CVD processes for ULSI usage in order to clarify the step coverage behavior of these processes systematically.

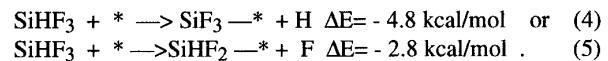
3. Analysis

The seven CVD processes examined included, W metal, polysilicon, silicon dioxide, and silicon nitride (Table I). We used molecular orbital theory to clarify the deposition scheme in those cases that lacked a clear reaction mechanism. One of the two W-CVD processes, $WF_6 + SiF_4$, is described separately because for this process atomistic simulation was helpful in clarifying the step coverage characteristics.

W-CVD from WF_6 and SiH_4

Tungsten (W) can be deposited from WF_6 and SiH_4 through the chemical reaction $WF_6 + 2SiH_4 \rightarrow W + 2SiHF_3 + 3H_2$ [7]. The deposition conditions for good step coverage in filling contact holes and trenches have been difficult to attain for this CVD process [8]. As a result, step coverage is poor. Two process models have been proposed to explain this poor coverage. One model assumes that a reverse reaction occurs in the feature [9]. Good agreement between simulated and experimental profiles has been reported when the reverse reaction rate is proportional to the product gas concentration [9]. The other model assumes that the product gas causes surface-site blocking [8]. This model is based on the experimental result that adding the product gas $SiHF_3$ reduces the film growth rate. Although both reaction models can explain phenomenologically the poor step coverage characteristic, a more convincing reaction model, especially of the inhibition mechanism, is needed to carry out accurate profile simulations. For this purpose, we previously examined the dissociative adsorption mechanism of product gas $SiHF_3$ and its energetics by using the ab initio molecular orbital program HONDO7 at the Hartree-Fock calculation level [10]. Details of our calculations were previously reported [11].

The initial dissociative reaction step on an active-site (*) of a W-growth surface can take two forms:



Both dissociation reactions are exothermic ones. For reaction (4), its succeeding dissociation reaction is calculated to be highly endothermic and does thus not readily occur. Reaction (5) can yield another dissociated species, $SiHF$; exothermically $\Delta E = -12.4 \text{ kcal/mol}$. Because $SiHF_3$ is thought to take dissociative path (4) preferentially over path (5), overall dissociation of $SiHF_3$ ends at its initial stage; there is no multiple dissociation. With this dissociation and active-site-blocking of the W surface, the deposition-rate expression for W-CVD can be readily derived,

$$R_w = K_1 P_{SiH_4} / (1 + K_2 \text{SQRT}(P_{SiHF_3})) \quad (6)$$

where P_{SiH_4} and P_{SiHF_3} are the local partial pressures of SiH_4

and SiHF_3 , respectively. To estimate kinetic parameters K_1 and K_2 , we used experimental data [8]. Using this rate expression, we simulated the step coverage characteristic at 637 K, $P_{\text{SiH}_4} = 25$ mTorr, and $P_{\text{WF}_6} = 45$ mTorr. Comparison of the experimental and simulated deposition profiles for a trench with an aspect ratio of 1.3 is shown in Fig. 3. The experimentally observed poor step coverage is well reproduced with this deposition model. This poor step coverage is not caused by depletion of the source gases in the trench, as shown in Fig. 4 which shows the flux distribution of the constituent gases. From the top to the bottom of the trench wall, the decrease in the source gas flux was very small. This indicates there was no depletion of the source gases associated with a deposition reaction and also there was no shadowing effect caused by the trench shape. On the other hand, a larger flux change along the trench side wall was observed for both product gases, almost one and half times larger at the bottom than at the top. This stagnation of product gases enhances the inhibition of deposition through dissociative adsorption and leads to poor step coverage. For this simulation, the reactive sticking coefficient of source gas WF_6 , evaluated outside the feature mouth was 5.7×10^{-3} , which

produces conformal coverage if we assume a commonality of sticking coefficients for determining the role of step coverage characteristics [5]. For the W-CVD from WF_6 and SiH_4 , we can conclude that the experimentally observed poor step coverage characteristic is due to active-site-blocking on the growing W surface caused by dissociative adsorption of the product gas, and that the reactive sticking coefficient is not a proper measure for predicting step coverage characteristics.

Other CVD Systems

The other six CVD systems we examined with our deposition simulator were W film from WF_6 and H_2 , polySi from SiH_4 , P-doped polySi from SiH_4 and PH_3 , SiO_2 from SiH_4 and N_2O , SiO_2 from tetraethoxysilane (TEOS), and Si_3N_4 from SiCl_2H_2 and NH_3 . The step coverage characteristics of these CVD systems in filling trenches with different aspect ratios from 1 to 5 were rigorously simulated and compared with the experimental profiles. The predicted film profiles for these CVD systems are shown in Fig. 5. The simulation conditions (gas pressures and deposition temperatures) were set at the experimental values described in the literature [12,13,14,15,16,17]. Molecular orbital calculations were also carried out to examine the reported deposition mechanism from the atomistic point of view, as was done in the case of W-CVD from WF_6 and SiH_4 . The molecular orbital simulation results for the reaction mechanism will be published elsewhere [18]. The reaction-rate expressions described in the literature were used as a first approximation because there were few discrepancies between the reported models and the models deduced from atomistic reaction modeling. The calculated deposition profiles agreed

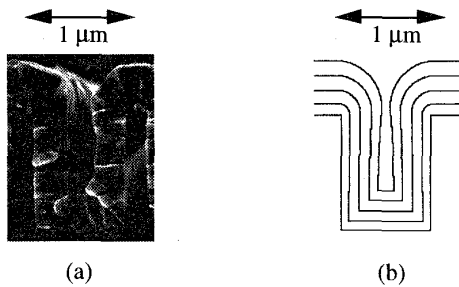


Fig.3 Comparison of experimental with simulated deposition profile for a trench with an aspect ratio of 1.3 : (a) experimental LPCVD profile of W from WF_6 and SiH_4 ; (b) simulated profile evolution.

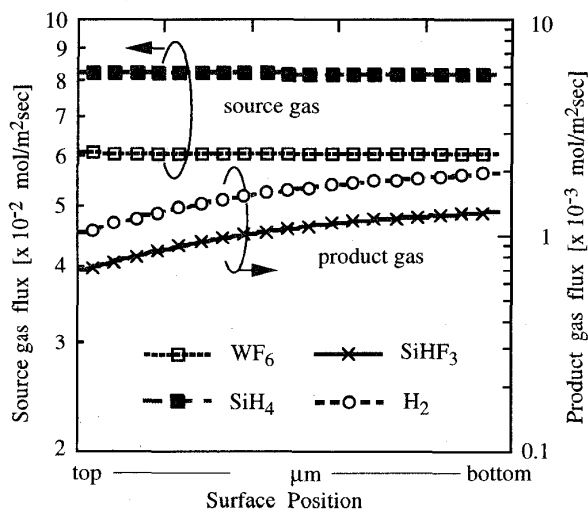


Fig.4 Flux distribution of source gases and product gases along the wall of trench feature shown in Fig. 3.

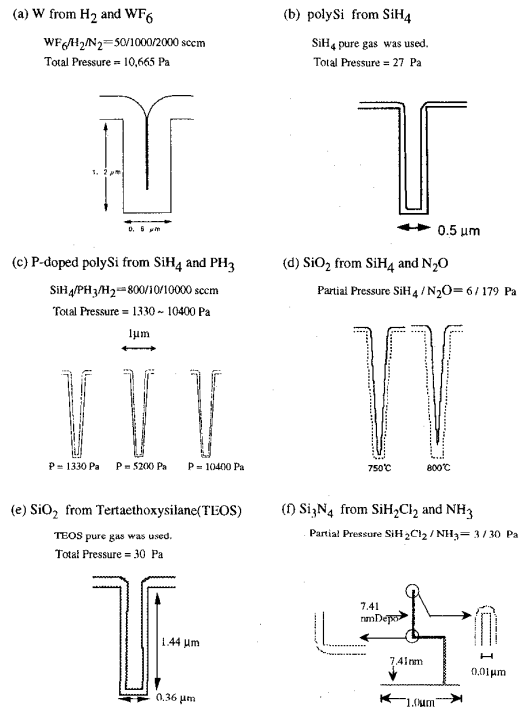


Fig. 5 Simulated deposition profiles for several CVD systems of ULSI usage with feature-scale deposition simulator described in text.

well with the experimental profiles; poor step coverage characteristics were obtained for the P-doped polySi film and the SiO₂ film from TEOS precursor, and relatively conformal step coverage characteristics were obtained for the other four systems. The reactive sticking coefficients of these systems were also evaluated outside the feature mouth. They are shown in Table I, along with the reaction-rate expressions used in the profile simulations. The evaluated reactive sticking coefficients for P-doped polySi and SiO₂ from TEOS, 6.8×10^{-6} and 2.9×10^{-7} , indicate that the sticking coefficient is an inadequate or rather confusing descriptor of the step coverage characteristics in profile simulation. It is thus highly risky for a process engineer to use the step coverage characteristics derived using the sticking coefficient. It is necessary to go back to the intrinsic reaction mechanism to understand all of the CVD characteristics; kinetics, coverage, film quality, and so on. To achieve a good intrinsic reaction mechanism, atomistic simulation based on molecular orbital theory is extremely useful, as demonstrated for W-CVD from WF₆ and SiH₄.

4. Conclusions

We have extended the two-dimensional deposition simulator with a micrometer feature scale and based on the ballistic transport and reaction model that was originally developed by Cale et al. to include a scheme to inhibit and/or accelerate the deposition reaction stemming from the product gases. We have also improved the algorithm used to calculate a self-consistent gas flux distribution on micro feature at each step in the simulation. Application of this deposition simulator to seven CVD systems for ULSI usage showed good agreement between the calculated and experimental feature profiles. The validity of the reactive sticking coefficient's role as a general

descriptor for step coverage characteristics was thoroughly examined using these simulated results and we concluded that the intrinsic reaction mechanism is more reliable than the sticking coefficient for all CVD characteristics. Molecular orbital calculation was also demonstrated to be extremely helpful in clarifying the intrinsic deposition mechanism.

Acknowledgments

We are grateful to Dr. Hisako Sato and Dr. Hiroo Masuda of Hitachi's Device Development Center, and to Dr. Masato Ikegawa and Mr. Nobuyuki Mise of Hitachi's Mechanical Research Laboratory for their useful discussion.

References

1. M. J. Cooke and G. Harris, *J. Vac. Sci. Technol.*, **A7**, 3217 (1989).
2. A. Yuuki, Y. Matsui, and K. Tachibana, *Jpn. J. Appl. Phys.*, **28**, 212 (1989).
3. S. Chatterjee and C. M. McConia, *J. Electrochem. Soc.*, **137**, 328 (1990).
4. T. S. Cale and G. B. Raupp, *J. Vac. Sci. Technol.*, **B8**, 1242 (1990).
5. M. K. Jain, T. S. Cale, and T. H. Gandy, *J. Electrochem. Soc.*, **140**, 242 (1993).
6. H. C. Wulu, K. C. Saraswat, and P. McVittie, *J. Electrochem. Soc.*, **138**, 1831 (1991).
7. N. Kobayashi, H. Goto, and M. Suzuki, *J. Appl. Phys.*, **69**, 1013 (1991).
8. C. A. Jeugd, N. Kobayashi, and H. Goto, in *Advanced Metallization for ULSI Applications*, p.369, Conference Proceedings ULSI-IX, Materials Research Society (1993).
9. T. S. Cale, G. T. Gandy, M. K. Jain, G. B. Raupp, M. Govil, and A. Hasper, in *Advanced Metallization for ULSI Applications*, p.101, Conference Proceedings ULSI-VII, Materials Research Society (1992).
10. HONDO7: *Quantum Chemistry Program Exchange #544*, Indiana University, Bloomington, IN., USA (1987).
11. Y. Takemura, J. Ushio, T. Maruizumi, R. Irie, and N. Kobayashi, in *Extended Abstract of the 1995 International Conference on Solid State Devices and Materials*, S-IV-2, p.73, The Japan Society of Applied Physics, Tokyo, 1995.
12. J. J. Hsieh and R. V. Joshi, in *Advanced Metallization for ULSI Applications*, p.77, Conference Proceedings ULSI-VII, Materials Research Society (1992).
13. R. J. Buss, P. Ho, W. G. Breiland, and M. E. Coltrin, *J. Appl. Phys.*, **63**, 2808 (1988).
14. H. Kurokawa, *J. Electrochem. Soc.*, **129**, 2620 (1982).
15. A. J. Learn and R. B. Jackson, *J. Electrochem. Soc.*, **132**, 2975 (1985).
16. G. B. Raupp, F. A. Shemansky, and T. S. Cale, *J. Vac. Sci. Technol.*, **B10**, 2422 (1992).
17. P. Pan and W. Berry, *J. Electrochem. Soc.*, **132**, 3001 (1985).
18. T. Maruizumi, J. Ushio, Y. Takemura, and M. Miyao (to be submitted).

Table I Thermal CVD processes examined using profile simulator described in text.

Film	Source	Reaction-rate expression	Reactive sticking coefficient (σ)		
			gas	σ	Temp.(K)
W	WF ₆ SiH ₄	$\frac{K_1 P_{SiH_4}}{1 + K_2 (P_{SiHF_3})^{1/2}}$	WF ₆	5.7×10^{-3}	623
W	WF ₆ H ₂	$\frac{1}{1/K_1 (P_{H_2})^{1/2} + 1/K_2 P_{WF_6}}$	WF ₆	6.7×10^{-4}	748
poly Si	SiH ₄	$K_1 P_{SiH_4}$	SiH ₄	1.4×10^{-3}	913
P-doped poly-Si	SiH ₄ PH ₃	$\frac{K_1 P_{SiH_4}}{1 + K_2 P_{SiH_4} + K_3 P_{PH_3}}$	SiH ₄	6.8×10^{-6}	923
SiO ₂	SiH ₄ N ₂ O	$K_1 P_{SiH_4} K_2 P_{N_2O}^5$	SiH ₄	1.5×10^{-5}	1023
SiO ₂	TEOS*	$\frac{K_1 P_{TEOS}}{1 + K_2 P_{TEOS}}$	TEOS	2.9×10^{-7}	1023
Si ₃ N ₄	SiCl ₂ H ₂ NH ₃	$K_1 + K_2 P_{SiCl_2H_2} / P_{NH_3}$	SiCl ₂ H ₂	5.4×10^{-5}	1043

* TEOS: Tetra Ethoxy Silane